JOURNAL OF ENGINEERING SCIENCES

Volume 11, Issue 2 (2024)

Veeranaath V., Dinesh S. G., Natarajan G. (2024). Multi-performance optimization of the mechanical characteristics of basalt fiber and silicon carbide-filled aluminum matrix composites. Journal of Engineering Sciences (Ukraine), Vol. 11(2), pp. C1–C12. https://doi.org/10.21272/jes.2024.11(2).c1

Multi-Performance Optimization of the Mechanical Characteristics of Basalt Fiber and Silicon Carbide-Filled Aluminum Matrix Composites

Veeranaath V.*[0000-0002-0056-9841], Dinesh S.G., Natarajan G.

Department of Mechanical Engineering, SRM Institute of Science and Technology, Kattankulathur, Chennai 603203, India

Article info:

Submitted:	April 3, 2024
Received in revised form:	July 5, 2024
Accepted for publication:	July 24, 2024
Available online:	August 5, 2024

***Corresponding email:**
veeranav@srmist.edu.in

Abstract. In the existing state, aluminum metal matrix composites (AlMMCs) are a category of materials that have successfully fulfilled the majority of demanding requirements in applications where moderate strength, high stiffness, and lightweight are necessary. This paper is focused on processing aluminum hybrid composites by reinforcing the aluminum alloy with a novel combination of fillers: basalt fibers and silicon carbide via stir casting. The main aim is to study the impact of processing conditions on the properties of the developed composite. Nine samples are produced by varying the reinforcement content, stirring rate, and duration based on the L9 Taguchi Array. SEM analysis is utilized to examine the microstructure of the developed composites. The samples were also machined and tested for their mechanical, physical, and wear behavior as per ASTM standards. The maximum density and hardness of 2883.3 kg/m^3 and 45.6 HRB, respectively, are observed at higher filler content conditions. In contrast, the minimum specific wear rate, maximum ultimate tensile, and impact strength of $1.86 \cdot 10^{-5}$ mm^3/(N·m), 263.5 MPa, and 93 N/mm are observed in higher stirring duration conditions. So, to avoid conflicting combinations of optimal input factors, grey relational analysis (GRA) tied with principle component analysis (PCA) is employed to determine the multi-objective performance parameter and the optimal combination of input factors for better response. Confirmatory tests were also performed to verify and validate the same. ANOVA analysis is also utilized to assess the significance of the process parameters on the responses.

Keywords: hybrid composites, stir casting, mechanical characterization, grey relational analysis.

1 Introduction

Today's technological applications require more robust, lighter, and cost-effective materials. The current focus is on developing materials with good power about weight. Ratios for automotive applications, where energy efficiency and increased engine response are becoming increasingly important, are an excellent example [1]. It has been observed that MMCs provide the customized property mixtures needed in various technical situations. Improved specific endurance, low thermal behavior, strong thermal insulation, good dampening capacity, exceptional resilience to wear, high specific rigidity, and corrosion resilience are a few of these attribute combinations [2]. MMCs were initially developed utilizing a single type of reinforcement filled in it. Hybrid MMCs are created by employing several reinforcing fillers in response to market demand and advancements. Hybrid MMCs exhibit improved mechanical properties owing to a reduction in semilunar cartilage immersion defects and a drop in the production of intermetallic components at surfaces owing to an increase in the interfacial area [3]. The subsequent sections confer the literature on aluminum-based compositions and improvements in their characteristics.

2 Literature Review

Siddharth Srivastava et al. [4] developed an aluminum hybrid MMC including WC, SiC, alumina, and rice shell ash at various weight proportions utilizing the Two-Stage Stir Casting technique. Assessment of density and mechanical possessions like impact and tensile strength revealed a linear relationship with the quantity of reinforcement. Microstructural examination revealed evenly spaced and uniformly dispersed SiC particulates

within the aluminum metal matrix. An enhancement in the mechanical characteristics of the formed composite was noted as a consequence of the appropriate dispersion of SiC.

Saravanan et al. [5] successfully employed stir casting to create hybrid MMCs based on aluminum. After utilizing a pin-on-disc device, the tribological performance of the MMCs was examined. In comparison to basic metal, composite materials have shown improved qualities such as hardness, ultimate tensile strength (UTS), and impact strength. The rise in filler content enhanced these qualities. For the 3 % wt. sample, the highest tensile strength was 173 MPa. Using SEM pictures, the abrasive wear process was also investigated.

Pitchayyapillai et al. [6] reinforced alumina and molybdenum disulfide in the aluminum matrix. They found that alumina particle weight increases the mechanical properties of hybrid composites, while MoS2-reinforcing fillers reduce hardness and UTS. For Al/alumina, aluminum oxide reinforcements improve wear resistance; In Al/Al_2O_3 composites, MoS_2 fillers with hybrid reinforcement improve wear and friction resistance.

Ravi Butola et al. [7] suggested that the hardness of commonly obtainable Al base is improved by including SiC and ash fillers; banana and coconut ash also have a similar effect. Bagasse has lower rigidity. The UTS increases with banana and coconut ash fillers, but the ductility decreases. Although the hardness or yield strength hardly increases and the UTS decreases, sugarcane ash retains its ductile quality.

Asif et al. [8] suggested that wear rates are lowered using graphite particulates in an aluminum matrix instead of SiC-strength composites. Friction coefficients are stabilized for sliding speeds and loads using solid fluids. Noise levels are decreased by adding solid ingredients to aluminum powder. The suggested composites based on aluminum exhibit superior tribological properties compared to those based on metal.

Gnaneswaran et al. [9] conducted experiments on hybrid MMCs based on LM6-Al material, which were manufactured with varying weight percentages of fillers. Suitable contact interconnections were seen in the microstructure, and hardness rose as the short fibers and fillers in the base matrix rose. With excellent strength noted for 5 weight percent of fiber-reinforced composite materials, UTS rose with the percentage of fiber fillers. The aluminum-based MMCs formed by stir casting at different stirring rates, stirring times, and proportions of the weight of SiC particle and MoS_2 particle were examined for their microstructure, hardness, UTS, and wear behavior. Compared to the Al-SiC composite, the Al-SiC–MoS_2 mixtures showed superior improvements in hardness, UTS, and wear resistance, showing increased wetting [10].

Kumar et al. [11] fabricated hybrid composites by filling glass powder particulates and shell ash in Al base, wherein an increment in UTS was observed due to increased dislocation density. Alumina with an Al base is improved mechanically and tribologically by adding graphite or SiC [12]. The material exhibited an exceptional UTS, ultimate compression strength, and high hardness. It has the best resistance to wear as well. Hybrid composites exhibit greater exterior micro-hardness because they contain reinforcement particles that reinforce grain boundaries and inhibit dislocation motion. As an outcome, tribological effectiveness was 30 % better than base metal hybrids [13].

Ng et al. [14] reinforced natural leaves and glass fiber in Al base and detected an improvement in UTS and flexural properties by 39 % and 21 %, respectively, due to its hybridization and balance. Critical failure mechanisms and crashworthiness performance are pointedly impacted by the hybridization process [15] and the rise in filler content, increasing the energy absorbed. When comparing composites with hybrid fillers to those with single fillers, there is a discernible improvement in mechanical characteristics. This is because hybrid reinforcement improves the spatial arrangement of each ceramic phase, which benefits each ceramic separately [16].

Shahabaz et al. [17] detected that the ultrasonication route was found to be the best technique for homogeneously dispersing the fillers in Al base, which in turn led to the development of solid bonds, which is the root cause for the improvement of characteristics of composites. Similarly, the composites with B_4C and SiC fillers exhibited resilience to dislocation movement, and finely tuned grains produced hardness values that were 21 % greater than those of a pure aluminum matrix [18]. SiC and B_4C reinforcements considerably raised the compressive strength of AMCs. The impact of SiC and B_4C particles was dependent on the hybrid composites' densities. Wear resilience was increased through the combinatorial impact of reinforcement particulates. The aluminum alloy melt that was stir-casted with fly ash and titanium diboride reinforcing fillers added showed better mechanical and density characteristics, including a clean interface and homogeneous dispersion [19].

Hybrid composites also exhibited decreased electrical conductivity, particularly in the presence of boron nitride and vanadium carbide particulates, owing to impairments in the motion of electrons within the base [20].

From the above literature review, it is apparent that Aluminum MMCs that have hybrid fillers are being applied in many ways and could address the present demand for sophisticated engineering components. The microstructures of hybrid composites, made using various reinforcing particles, are uniformly distributed and exhibit stability. Powder metallurgy and stir casting are prevalent methods. Incorporating hard fillers, ceramic fillers, and graphite as an additional filler can increase the strength of the composite. Agro waste derivatives, such as fly ash, rice husk ash, and coconut shell ash, can be used for extra reinforcement in the forthcoming generations of hybrid composites [21].

Hence, this paper develops aluminum hybrid composites through stir casting to reinforce the aluminum alloy with a novel combination of fillers, namely silicon carbide and basalt fibers. Nine samples are generated by adjusting the reinforcement content, stirring rate, and duration by the L9 Taguchi Array. The microstructure of

the created composites is examined using SEM analysis. After machining, the samples underwent mechanical, physical, and wear behavior testing by ASTM standards.

3 Research Methodology

Aluminum alloy (Al 6061) is employed as the matrix material in the paper, the chemical composition of which is given in Table 1. Due to Al 6061's low weight, affordability, and excellent formability and weldability, it is widely utilized. Silicon carbide (SiC) powdered particulates (40–60 μm) fillers were employed to manufacture this composite, which certainly increases the composites' features. Basalt fibers (diameter 10–25 μm and length 2–4 mm) were also used as secondary fillers to develop specimens.

Table 1 – Chemical composition of Al 6061 alloy

Element	Si	Zn	Cr	Fe	Cu	Al
Composition, %	0.5	0.1	0.2	0.3	0.2	Balance

Stir casting setup and Al-based hybrid MMCs are presented in Figure 1.

a b

Figure 1 – Stir casting setup (a) and Al-based hybrid MMCs (b)

The stir casting setup using liquid metallurgy was used to create the Al 6061 alloy-based hybrid MMCs, as seen in Figure 1a. 900 g of Al 6061 alloy was liquified in a graphite crucible and heated up to 700 °C. Then, the SiC and basalt fibers were preheated and stirred by employing a motorized stirring setup at varying filler content, stirring rates, and duration, as displayed in Tables 2, 3. The stirring process causes the impeller to exert shear force, which splits basalt and SiC fibers. The melt is constantly agitated to guarantee that the ceramic fibers and particles are evenly distributed throughout the matrix.

Thus, to create the samples illustrated in Figure 1b, the melted melt is poured into a cast iron die preheated to 250 °C and must be 200 mm long by 40 mm in diameter. As per ASTM standards, the specimens were machined for various physical and mechanical characterization.

Table 2 – Process parameters and their levels

Parameter	Unit	L1	L2	L3
Reinforcement, % wt.	%	1	2	3
Stirring speed	rpm	500	750	1000
Stirring duration	min	10	15	20

Table 3 – Design of experiments – L9 Taguchi array

Designation	Reinforcement, % wt.	Stirring speed, rpm	Stirring duration, min
C1	1	500	10
C2	1	750	15
C3	1	1000	20
C4	2	500	15
C5	2	750	20
C6	2	1000	10
C7	3	500	20
C8	3	750	10
C9	3	1000	15

Microstructural characterization of the developed composites was performed utilizing an optical microscope "Olympus – Upright". Archimedes' principle was used to calculate the samples' density experimentally. Archimedes' principle can be utilized to determine the composite's density by comparing its weight in the air to its weight when placed in a liquid, generally water. The density is determined using the following equation:

$$d_c = \frac{w_a}{w_a - w_w} \cdot d_w, \quad (1)$$

where d_c, d_w – densities of composite and water, respectively; w_a, w_w – weights of the composite in air and water, respectively.

Hardness is determined using the Rockwell Hardness Testing Machine at a load of 600 N, dwell time of 5 s, and 1/16-inch indenter. With the "Pin-On-Disc" device, wear tests are carried out. It is conducted at a 10 N load, sliding velocity of 2 m/s, and sliding distance of 750 m. The disc employed for testing is made of EN32, and the disc track diameter is 60 mm. The Tensometer, which has an area of cross-section of 12.54 mm^2, a load cell of 20 kN, a specimen length of 20 mm, and an evaluation rate of 1.0 mm/min, was utilized to accomplish tensile testing. Impact strength is determined using a Charpy impact testing machine with a 30^o angle of striking edge and a radius of curvature as 2.0–2.5 mm.

The optimal conditions for individual response of developed composites are different. So, to avoid conflicting input factors, grey relational analysis (GRA) tied with principle component analysis (PCA) is utilized to evaluate the multi-objective performance parameter and the optimal combination of input factors for better response. This technique converts multi-objective to single-objective optimization with a grey relational grade index. When paired with PCA, this technique has numerous applications in various fields, such as economics, ecological research, technology, and decision-making. The combination of principal component analysis and grey relational analysis is a powerful technique for assessing data and making decisions that increase interpretability, resilience, and efficiency in various scenarios. Confirmatory tests were also performed to verify and validate the same. ANOVA analysis is also exploited to evaluate the significance of the processing constrictions on the responses.

4 Results

4.1 Density

Table 4 gives the experimentally detected responses of the composites (Figure 2).

Table 4 – Physical and mechanical characterization

Exp. no.	Density, kg/m^3	HRB	Specific wear rate mm^3/(N·m) ×10^{-5}	UTS, MPa	Impact strength, N/mm
1	2764.5	33.2	0.143	187.0	80
2	2784.5	34.8	1.410	192.3	82
3	2798.6	34.6	1.669	210.2	83
4	2776.3	35.6	0.428	204.5	84
5	2798.3	35.7	0.392	221.3	83
6	2802.3	38.2	0.662	231.0	85
7	2883.3	41.2	0.438	241.2	91
8	2828.5	45.6	0.186	232.5	93
9	2813.2	44.8	0.196	263.5	92

The density of the developed composites was measured experimentally by employing Archimedes' principle.

Figure 3 exhibits the contour plot of the consequence of processing constraints on the density of the composites. Compared with other process parameters, this property of the composites is found to rise with a rise in filler content due to the addition of highly dense filler particulates and the absence of gas entrapping.

ANOVA analysis is carried out at a 95 % confidence interval level to yield a model R^2 value of 84.90 %, as depicted in Table 5. It again confirms that the most significant parameter with a contribution of 62.0 % is reinforcement content in the base matrix.

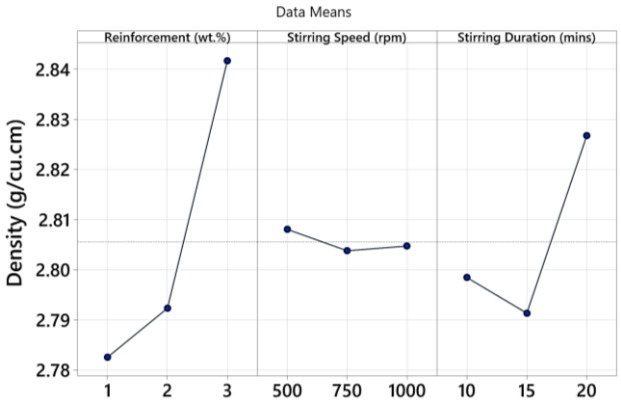

Figure 2 – Main effect plot: density, `3

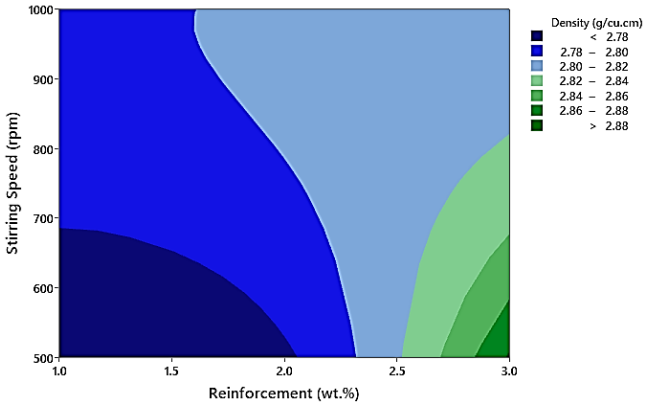

a

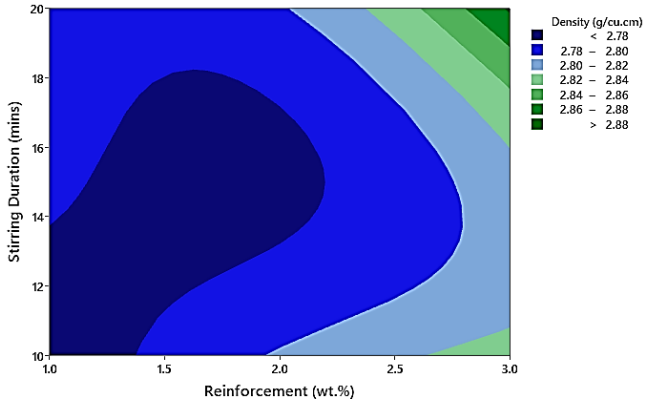

b

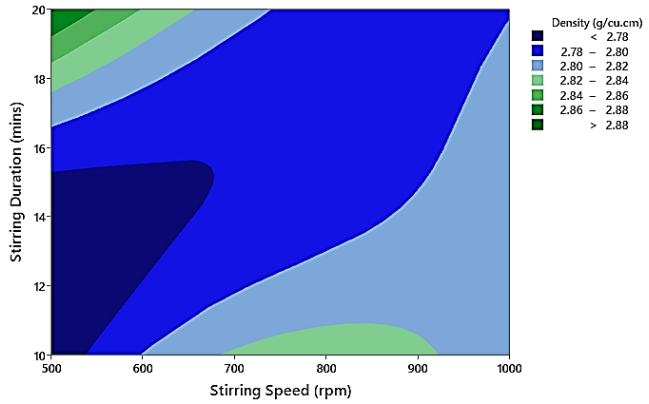

c

Figure 3 – Density vs. stirring speed and reinforcement (a), stirring duration and reinforcement (b), and stirring duration and stirring speed (c)

Table 5 – ANOVA analysis: density

Source	DF	Seq. SS	Contribution, %	Adj. SS	Adj. MS	F-value	P-value
Reinforcement, % wt.	2	0.006029	61.99	0.006029	0.003015	3.86	0.206
Stirring speed, rpm	2	0.000030	0.310	0.000030	0.000015	0.02	0.981
Stirring duration, min	2	0.002104	21.64	0.002104	0.001052	1.35	0.426
Error	2	0.001562	16.06	0.001562	0.000781	–	–
Total	8	0.009725	100.0	–	–	–	–

4.2 Hardness

The hardness is measured in three measurements taken on each sample to ensure uniformity, and the average value was determined as the hardness of the composite, as shown in Table 4.

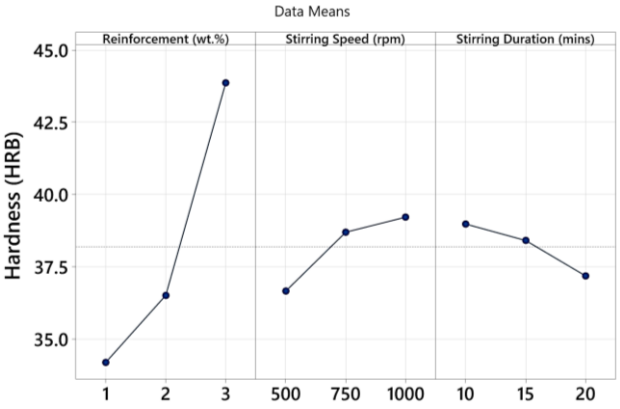

Figure 4 – Main effect plot: hardness

From Table 4, it is understandable that reinforcements in the matrix are the most influential parameter of hardness.

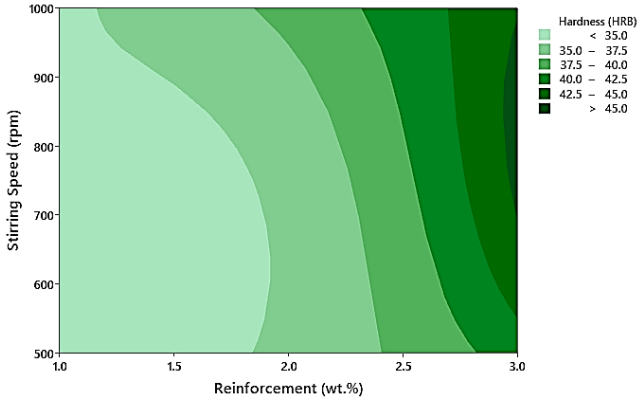

a

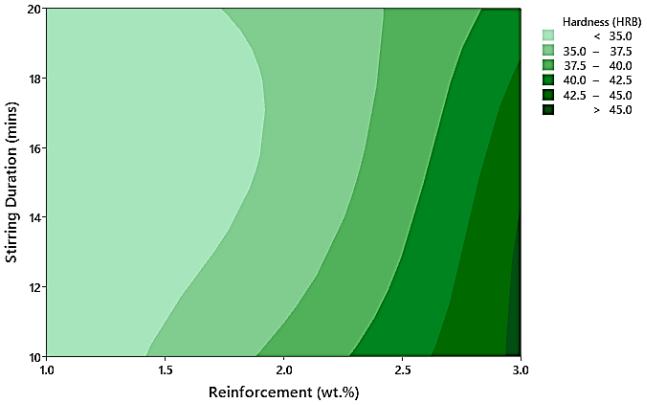

b

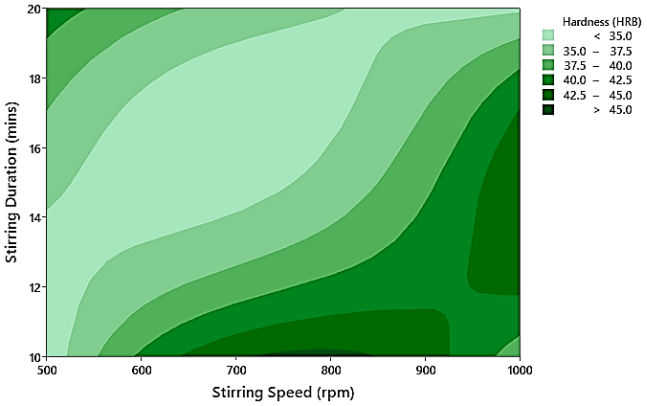

c

Figure 5 – Hardness vs. stirring speed and reinforcement (a), stirring duration and reinforcement (b), and stirring duration and stirring speed (c)

ANOVA analysis is carried out at a 95 % confidence interval level to yield a model R^2 value of 99.55 %, as depicted in Table 6. It again confirms that the most significant parameter with a contribution of 90.1 % is reinforcement content in the base matrix.

Table 6 – ANOVA analysis: hardness

Source	DF	Seq. SS	Contribution, %	Adj. SS	Adj. MS	F-value	P-value
Reinforcement, % wt.	2	153.027	90.12	153.027	76.5136	201.3	0.005
Stirring speed, rpm	2	10.955	6.450	10.955	5.4775	14.41	0.065
Stirring duration, min	2	5.0580	2.980	5.058	2.5288	6.650	0.131
Error	2	0.7600	0.450	0.760	0.3801	–	–
Total	8	169.80	100.0	–	–	–	–

4.3 Wear test

The composites' specific wear rate (SWR) is evaluated and given in Table 4. However, Figure 6 shows that fillers in the matrix are the most influential parameter of the specific wear rate.

The minimum SWR of $1.43 \cdot 10^{-5}$ $mm^3/(N \cdot m)$ is detected. As the filler amount in the matrix rises, the SWR of the synthesized samples decreases considerably because of the upsurge in the hardness of the samples, as more hardened samples resist more wear and are less prone to abrasive wear.

Figure 7 exhibits the contour plot of the consequence of processing constraints on the SWR of the composites.

ANOVA analysis is carried out at a 95 % confidence interval level to yield a model R^2 value of 74.00 %, as depicted in Table 7. It again confirms that the most significant parameter with a contribution of 42.0 % is reinforcement content in the base matrix.

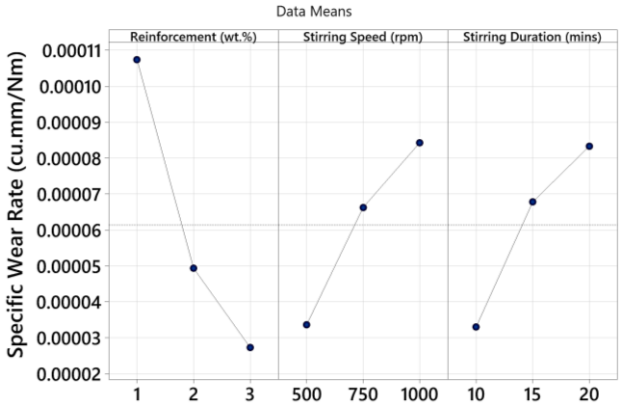

Figure 6 – Main effect plot: SWR

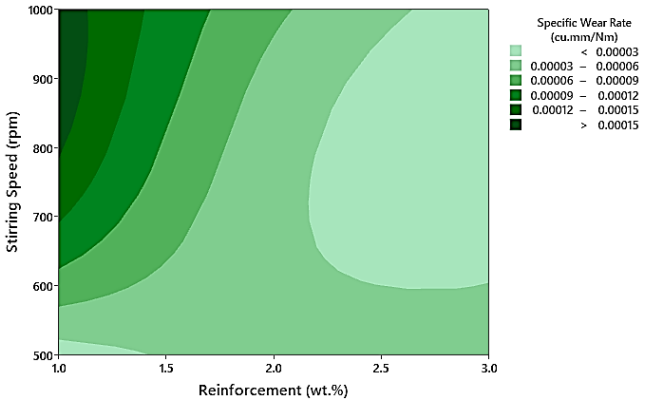

a

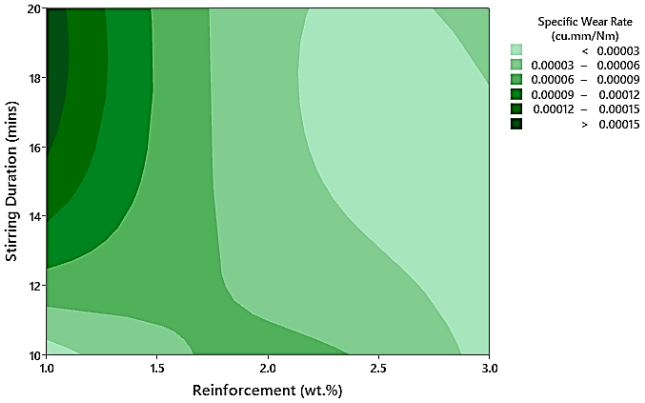

b

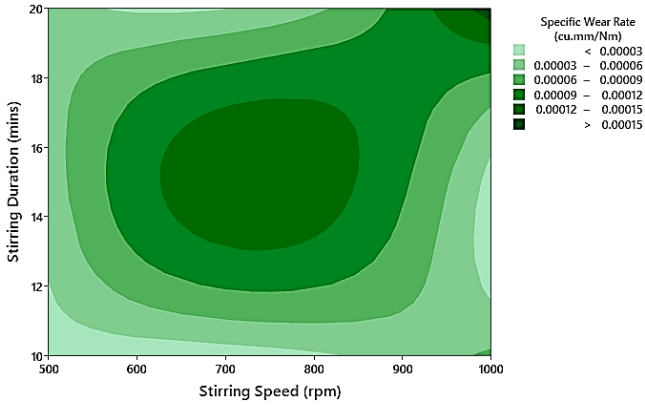

c

Figure 7 – SWR vs. steering speed and reinforcement (a), stirring duration and reinforcement (b), and stirring duration and stirring speed (c)

Table 7 – ANOVA analysis: SWR

Source	DF	Seq. SS	Contribution, %	Adj. SS	Adj. MS	F-value	P-value
Reinforcement, % wt.	2	0.000000	42.00	0.000000	0.000000	1.64	0.379
Stirring speed, rpm	2	0.000000	16.15	0.000000	0.000000	0.63	0.613
Stirring duration, min	2	0.000000	16.27	0.000000	0.000000	0.64	0.611
Error	2	0.000000	25.58	0.000000	0.000000	–	–
Total	8	0.000000	100.0	–	–	–	–

4.4 Tensile test

The composites' UTS is evaluated and given in Table 4. Also, Figure 8 shows that fillers in the matrix are the most influential parameter of UTS.

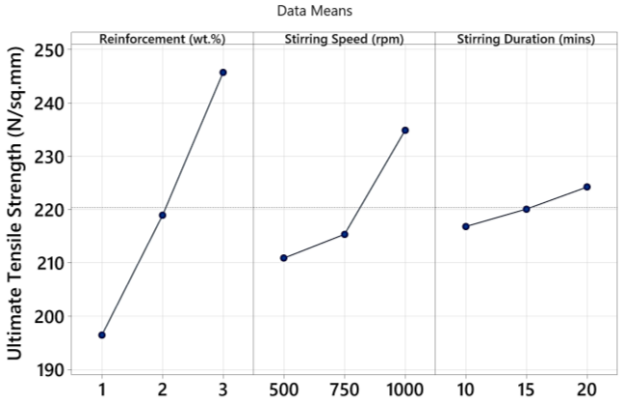

Figure 8 – Main effect plot: UTS

The maximum UTS of 263 MPa is detected. As the filler content in the matrix rises, the UTS of the fabricated samples increases considerably because of the upsurge in the yield strength of the samples as these samples resist more elongation and are less prone to failure easily.

Figure 9 exhibits the contour plot of the consequence of processing constraints on the UTS of the composites.

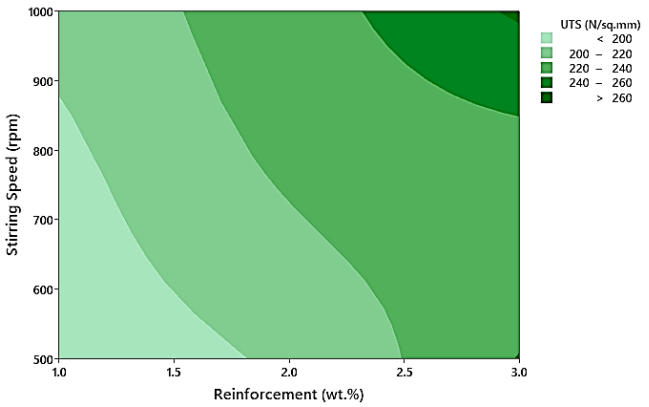

a

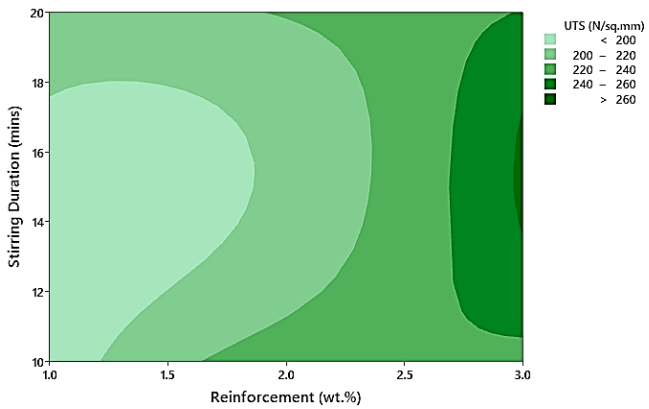

b

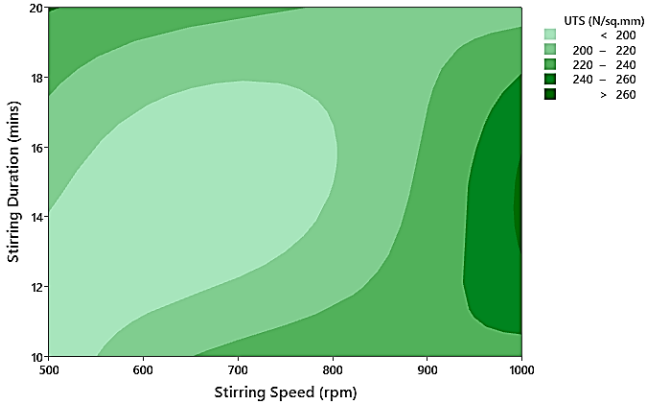

c

Figure 9 – UTS vs. stirring speed and reinforcement (a), stirring duration and reinforcement (b), and stirring duration and (c) stirring speed

ANOVA analysis is carried out at a 95 % confidence interval level to yield a model R^2 value of 97.79 %, as depicted in Table 8. It again confirms that the most significant parameter with a contribution of 75.8 % is reinforcement content in the base matrix.

Table 8 – ANOVA analysis: UTS

Source	DF	Seq. SS	Contribution, %	Adj. SS	Adj. MS	F-value	P-value
Reinforcement, % wt.	2	3645.4	75.76	3645.4	1822.7	34.26	0.028
Stirring speed, rpm	2	977.50	20.31	977.50	488.75	9.190	0.098
Stirring duration, min	2	82.520	1.710	82.520	41.260	0.780	0.563
Error	2	106.42	2.210	106.42	53.210	–	–
Total	8	4811.9	100.0	–	–	–	–

4.5 Impact test

The impact strength of the composites is evaluated and given in Table 4. Also, Figure 10 shows that fillers in the matrix are the most influential parameter of this property. The maximum value of 93 N/mm is detected.

As the reinforcement content in the matrix rises, the same amount of the developed specimens increases considerably because of the inclusion of filler particulates in the matrix, improving the load transfer mechanism.

Figure 11 exhibits the contour plot of the consequence of processing constraints on this property of the composites.

ANOVA analysis is carried out at a 95 % confidence interval level to yield a model R^2 value of 97.72 % as depicted in Table 9. It again confirms that the most significant parameter with a contribution of 95.3 % is reinforcement content in the base matrix.

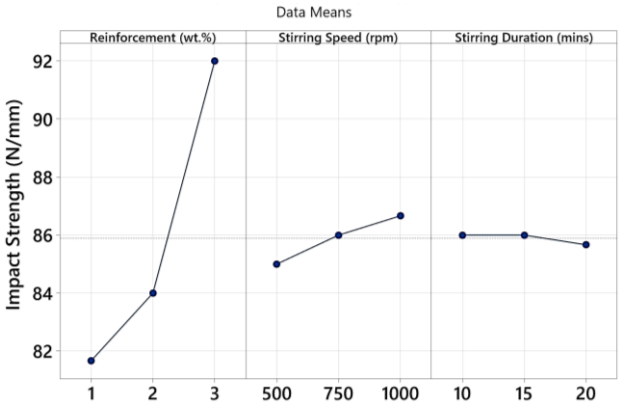

Figure 10 – Impact strength

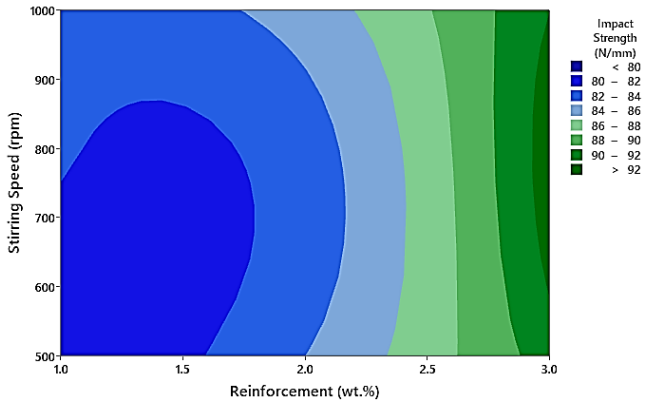

a

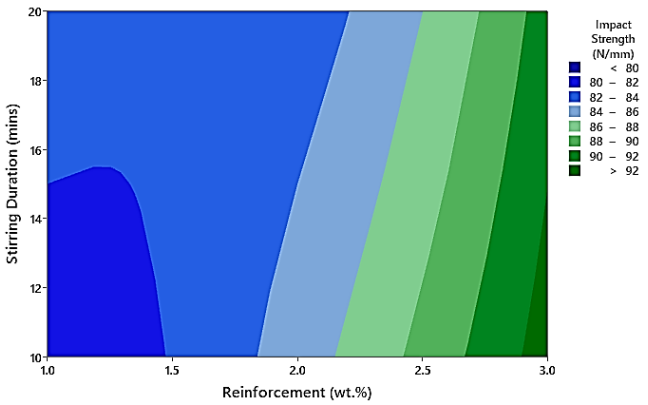

b

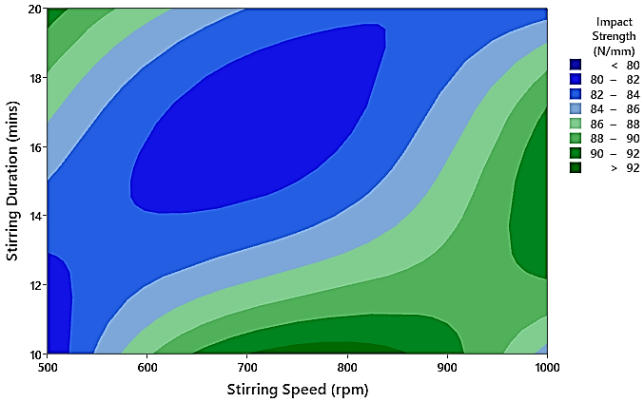

c

Figure 11 – Impact strength vs. stirring speed and reinforcement (a), stirring duration and reinforcement (b), and stirring duration and stirring speed (c)

Table 9 – ANOVA analysis: impact strength

Source	DF	Seq. SS	Contribution, %	Adj. SS	Adj. MS	F-value	P-value
Reinforcement, % wt.	2	176.22	95.31	176.2	88.111	41.7	0.023
Stirring speed, rpm	2	4.2220	2.280	4.222	2.1111	1.00	0.500
Stirring duration, min	2	0.2220	0.120	0.222	0.1111	0.05	0.950
Error	2	4.2220	2.280	4.222	2.1111	–	–
Total	8	184.89	100.0	–	–	–	–

4.6 Microstructure of composites

The fabricated specimens' microstructural characterization was tested using an optical microscope, as shown in Figure 12. Due to its ability to clarify the fundamental features and attributes linked to mechanical analysis, microstructural analysis is highly significant. Figure 12a shows that more porosity is observed at 1 % wt. filler content, which in turn lessens the composites' density, thereby affecting the fabricated samples' performance. It is also apparent from Figure 12a that the produced composite's surface has a lot of large craters. The released gases from the surroundings were the cause of the gas holes that were seen. It is also observed that the pores in composites are reduced with a rise in the filler content, thereby increasing the density, as shown in Figure 12b. It is also observed that grain refinement is initiated, which may cause the improvement of physical and mechanical characteristics. Further, grain refinement is observed at higher levels of filler content, increasing the properties to the maximum level (Figure 12c).

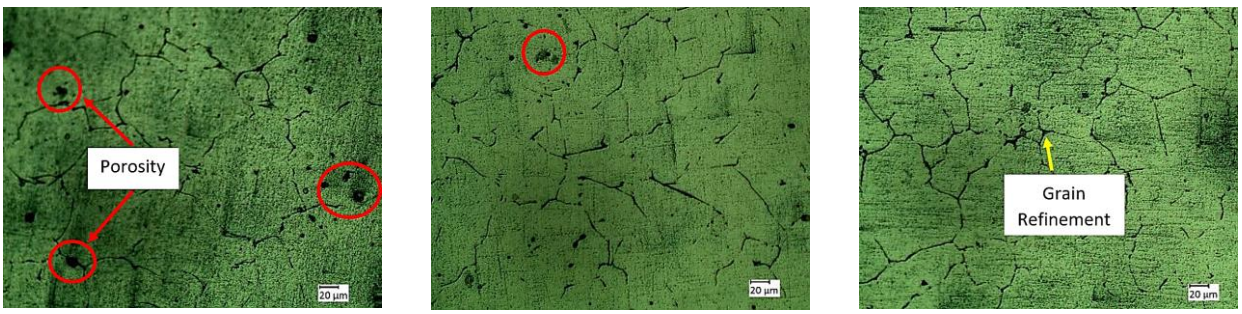

a b c

Figure 12 – Microstructure of composites with reinforcement content in the matrix: a – 1 % wt.; b – 2 % wt.; c – 3 % wt.

4.7 Optimization

Tied with PCA, GRA uses a concept known as grey, which illustrates the lack of ambiguous information, to optimize several output cases when the constraints are complex and unclear. Calculating the deviation and grey relational coefficient from which ranking is determined based on PCA weights and normalizing test results are all part of grey relation analysis.

Table 10 shows the results' GRA. It also displays the normalization of the test findings and the rank with grey relational grade (GRG), deviation, and grey relational coefficient, where C9 yields the best rank.

Table 10 – GRA: responses and normalization, deviation sequences, GRG, and ranking

Benefit	Non-Beneficial	Beneficial					
Weightage	0.131	0.056	0.321	0.155	0.335		
No.	SWR, $mm^3/(N·m)$	Density, kg/m^3	Hardness, HRB	UTS, MPa	Impact strength, N/mm		
1	0.0000143	2764	33.16	187.0	80		
2	0.0001410	2784	34.82	192.3	82		
3	0.0001669	2798	34.61	210.2	83		
4	0.0000428	2776	35.60	204.5	84		
5	0.0000392	2798	35.72	221.3	83		
6	0.0000662	2802	38.23	231.0	85		
7	0.0000438	2883	41.23	241.2	91		
8	0.0000186	2828	45.56	232.5	93		
9	0.0000196	2813	44.82	263.5	92		
Normalized values							
No.	SWR, $mm^3/(N·m)$	Density, kg/m^3	Hardness, HRB	UTS, MPa	Impact strength, N/mm		
1	1.000	0.000	0.000	0.000	0.000		
2	0.170	0.168	0.134	0.069	0.154		
3	0.000	0.287	0.117	0.303	0.231		
4	0.813	0.099	0.197	0.228	0.308		
5	0.837	0.284	0.206	0.448	0.231		
6	0.660	0.318	0.409	0.575	0.385		
7	0.807	1.000	0.651	0.708	0.846		
8	0.972	0.538	1.000	0.594	1.000		
9	0.965	0.409	0.940	1.000	0.923		
No.	Deviation sequences						
	SWR, $mm^3/(N·m)$	Density, kg/m^3	Hardness, HRB	UTS, MPa	Impact strength, N/mm		
1	0.000	1.00	1.000	1.00	1.000		
2	0.830	0.83	0.866	0.93	0.846		
3	1.000	0.71	0.883	0.69	0.769		
4	0.187	0.90	0.803	0.77	0.692		
5	0.163	0.71	0.793	0.55	0.769		
6	0.340	0.68	0.591	0.42	0.615		
7	0.193	0.00	0.349	0.29	0.154		
8	0.028	0.46	0.000	0.40	0.000		
9	0.035	0.59	0.059	0.00	0.077		
No.	Grey relational coefficient					GRG	Rank
	SWR, $mm^3/(N·m)$	Density, kg/m^3	Hardness, HRB	UTS, MPa	Impact strength, N/mm		
1	1.000	0.33	0.333	0.33	0.3333	0.42	7
2	0.376	0.37	0.365	0.34	0.3714	0.36	9
3	0.333	0.41	0.361	0.41	0.3939	0.38	8
4	0.728	0.35	0.383	0.39	0.4193	0.44	6
5	0.754	0.41	0.386	0.47	0.394	0.45	5
6	0.595	0.42	0.458	0.54	0.448	0.48	4
7	0.721	1.00	0.588	0.63	0.765	0.69	3
8	0.946	0.52	1.000	0.55	1.000	0.89	1
9	0.9350	0.45	0.893	1.00	0.8666	0.88	2

In Figure 13, the GRG's mean effects plot is displayed, giving the predicted optimal conditions of 3 % wt. reinforcement content, 1000 rpm sliding rate, and 10 min sliding duration to yield a better response.

Table 11 presents an ANOVA analysis of the GRG at a 95 % confidence interval level to yield a model R^2 value of 97.65 %.

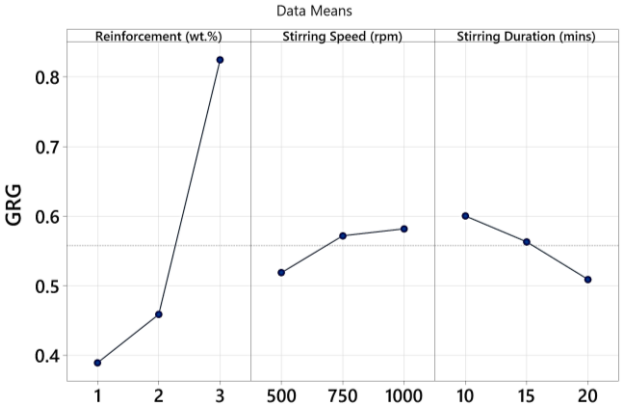

Figure 13 – Main effect plot: GRG

It again confirms that the most significant parameter with a contribution of 92.2 % is reinforcement content in the base matrix.

Confirmatory tests were also performed to verify and validate the same given in Table 12. The experimental and predicted values are detected and validated. An improvement of 0.11 is detected in the grey relational grade, which is the multiple characteristic indices of the composites.

Table 11 – ANOVA analysis: GRG

Source	DF	Seq. SS	Contribution, %	Adj. SS	Adj. MS	F-value	P-value
Reinforcement, % wt.	2	0.327513	92.20	0.327513	0.163756	39.24	0.025
Stirring speed, rpm	2	0.006873	1.930	0.006873	0.003436	0.82	0.548
Stirring duration, min	2	0.012617	3.550	0.012617	0.006309	1.51	0.398
Error	2	0.008347	2.350	0.008347	0.004174	–	–
Total	8	0.355350	100.0	–	–	–	–

Table 12 – Confirmatory tests

Response	Experimental (A3B2C1)	Prediction (A3B3C1)	Confirmatory experiment (A3B3C1)
SWR, $mm^3/(N \cdot m)$	$1.86 \cdot 10^{-5}$	$1.79 \cdot 10^{-5}$	$1.72 \cdot 10^{-5}$
Density, kg/m^3	2828	2831	2841
Hardness, HRB	45.56	47.23	46.23
UTS, MPa	232.5	228.3	235.1
Impact strength, N/mm	93	92	94
GRG	0.89	–	1
Improvement in GRG is 0.11			

5 Discussion

Figure 2 shows that fillers in the matrix are the most substantial parameter of density. The maximum density of 2883.3 kg/m^3 is detected at 3 % wt. filler content. As the filler content in the matrix rises, the same rises considerably because these filler particulates occupy the vacant sites in the matrix, decreasing the porosity and increasing the density. A decrease in density at a lower filler content could be credited to pores in the structure.

As shown in Figure 3, as the stirring speed increases from 500 rpm to 750 rpm, the density decreases as more gas is entrapped inside the composites, inducing more pores and voids. This may also be owing to the accumulation of the filler particles, which could be reduced with a further rise to 1000 rpm, thereby increasing the density [5].

Concerning stirring speed, the same trend is followed, wherein the decrease in density might also be due to particulate breakage, which is induced by higher shear forces at higher speeds. There might also be the formation of localized heat zones at higher speeds, which might degrade the characteristics [7].

Concerning stirring duration, the density is higher at 20 min of blending as prolonged stirring induced homogeneous dispersion of fillers in the base. Overall, the density is higher at higher levels of filler content, mid-level stirring rate, and high levels of durations.

From Figure 4, the maximum hardness of 45.56 HRB is detected at 3 % wt. filler content. As the filler content in the matrix rises, the same of the synthesized samples rises considerably because of the fillers' load-bearing ability and the specimens' increased density. Figure 5 exhibits the contour plot of the consequence of processing constraints on this property of the composites. Concerning other process parameters, the effect of filler content is more significant for hardness as it helps transfer the load from the base to the matrix. It is detected that this property of the developed samples is found to rise considerably with the rise in filler content due to the dislocation pinning, which means that these filler particulates may act as hindrances for the gliding of dislocations in the base, which in turn improves the hardness [8].

In addition, it was detected that hardness increases with increasing stirring speed, as at higher speeds, the accumulation of the filler particles is eliminated, resulting in an even distribution. It may also be due to the refinement

of microstructure and improved wettability. Hard-reinforced particles in the metal base of composite materials can prevent dislocation and displacement. Refinement of the microstructure results in a finer dispersion of these particulates, enhancing the pinning of dislocations and the component's hardness. On the contrary, the hardness declines with a rise in stirring duration as prolonged stirring may guide over-mixing, which may harm filler particulates and re-agglomerate fillers. Prolonged stirring may also lead to air bubbles or void formation in samples, thereby reducing the density of the specimens [10]. Overall, the hardness is detected to be better at higher filler content and stirring rate levels, as well as mid-level stirring durations.

From Figure 7, as the load-bearing ability is better with a rise in filler content, the developed composites can endure more contact stress, inducing less wear and decreasing SWR. This may also be due to lubrication retention, as some filler particles retain lubricant properties, which may reduce friction, resulting in a reduction in SWR [9].

It was also detected that SWR increases with increasing stirring speed, as at higher speeds, the re-agglomeration of the filler particles may be induced due to matrix degradation and poor bonding, thereby reducing the lubrication effect and increasing the wear. In a similar trend, the SWR is detected to increase with a rise in stirring duration as prolonger stirring may guide over-mixing, which may harm the filler particulates and re-agglomerate fillers. Prolonged stirring may also lead to air bubbles or void formation in samples, thereby reducing the density of the specimens and, in turn, inducing more wear [10]. Overall, the SWR is detected to be better at low filler content levels and low stirring rates and durations.

From Figure 9, as the load-bearing ability is improved with a rise in filler content, the developed composites can endure more contact stress, i.e., less failure and increasing UTS. The interfacial bond strength improved the composite's UTS because of the even distribution of filled particulates. It was also detected in [9].

In addition, it was detected that UTS increases with increasing stir rallying speed, as at higher speeds, the agglomeration of the filler particles may be avoided due to uniform dispersal of fillers and improved bonding.

Similarly, the UTS increases with a rise in stirring duration as prolonger stirring may induce better particle dispersion, thereby inducing even stress dispersion, enhanced wettability, and microstructure refinement [10]. Overall, the UTS is found to be better at low levels of filler content, stirring rate, and stirring durations.

From Figure 11, with a rise in filler content, the developed composites' ability to withstand load-bearing increases, leading to reduced failure rates and increased impact strength. The outcome of the impact testing is determined by the amount of energy engrossed by the material once subjected to an abrupt force [22]. In addition, it was detected that impact strength rises with increasing stirring speed, as at higher speeds, the agglomeration of the filler particles may be avoided due to the uniform dispersal of fillers and improved bonding. On the contrary trend, the impact strength is detected to decline with a rise in stirring duration as prolonger stirring may guide over-mixing, which may harm the filler particulates and re-agglomerate fillers [8]. Overall, the impact strength is detected to be better at low filler content and stirring rate levels and high levels of stirring durations.

Figure 12a shows that the air (gas) released during the stir-casting process is undeniably linked to the crater formed [11].

6 Conclusions

This paper is chiefly fixated on fabricating aluminum matrix hybrid composites by incorporating SiC and basalt fibers in the aluminum matrix utilizing the stir casting technique and its characterization.

The maximum density of 2883.3 kg/m^3 is determined at a filler content of 3 % wt. Compared to other process parameters, the density of composites increases with increasing filler content due to the insertion of high-density filler particles and the absence of gas inclusions.

The hardness of the developed samples is found to rise considerably with the rise in filler content due to the dislocation pinning, which means that these filler particulates may act as hindrances for the gliding of dislocations in the base that, in turn, improves the hardness.

The SWR is detected to be better at low filler content levels and low stirring rate and duration. Tensile and impact strength of the composites is detected to rise with a rise in filler content and stirring duration. Reinforcement is found to be the most significant parameter for all the responses when adding to the multiple characteristic index of the composites.

Grey relational analysis is employed to optimize the consequence of the various manufacturing constraints on the various output responses. The predicted optimal conditions are 3 % wt. reinforcement content, 1000 rpm sliding rate, and 10 min sliding duration to yield a better response. The experimental and predicted values are detected and validated via confirmatory tests. An improvement of 0.11 is detected in the grey relational grade, which is the multiple characteristic indices of the composites.

References

1. Bodunrin, M.O., Alaneme, K.K., Chown, L.H. (2015). Aluminum matrix hybrid composites: a review of reinforcement philosophies; mechanical, corrosion and tribological characteristics. *Journal of Materials Research and Technology*, Vol. 4(4), pp. 434–445. https://doi.org/10.1016/j.jmrt.2015.05.003
2. James, S.J., Ganesan, M., Santhamoorthy, P., Kuppan, P. (2018). Development of hybrid aluminum metal matrix composite and study of the property. *Materials Today: Proceedings*, Vol. 5(5(2)), pp. 13048–13054. https://doi.org/10.1016/j.matpr.2018.02.291

3. Muley, A.V., Aravindan, S., Singh, I.P. (2015). Nano and hybrid aluminum-based metal matrix composites: An overview. *Manufacturing Review*, Vol. 2, 15. https://doi.org/10.1051/mfreview/2015018
4. Srivastava, S., Malik, V., Bhatnagar, M.K., Verma, N., Mamatha, T.G., Vishnoi, M. (2021) Characterization of aluminium hybrid metal matrix composites. *Research Square*, Preprint. https://doi.org/10.21203/rs.3.rs-648677/v1
5. Saravanan, S., Sreenithi, A., Ajitha, M., Ilakkiyal, R., Narmatha, S.R., Rajkumar, S., Karthikeyan, K. (2020). Tribological behaviour of aluminum alloy (AA7075) based hybrid composites. *IOP Conference Series: Materials Science and Engineering*, Vol. 923, 012053. https://doi.org/10.1088/1757-899X/923/1/012053
6. Pitchayyapillai, G., Seenikannan, P., Raja, K., Chandrasekaran, K. (2016). Al6061 hybrid metal matrix composite reinforced with alumina and molybdenum disulphide. *Advances in Materials Science and Engineering*, Vol. 2016, 6127624. https://doi.org/10.1155/2016/6127624
7. Butola, R., Pratap, C., Shukla, A., Walia, R.S. (2019). Effect on the mechanical properties of aluminum-based hybrid metal matrix composite using stir casting method. *Materials Science Forum*, Vol. 969, pp. 253–259. https://doi.org/10.4028/www.scientific.net/MSF.969.253
8. Asif, M., Chandra, K., Misra, P.S. (2011). Development of aluminium based hybrid metal matrix composites for heavy duty applications. *Journal of Minerals & Materials Characterization & Engineering*, Vol. 10, pp. 1337–1344. https://doi.org/10.4236/jmmce.2011.1014105
9. Gnaneswaran, P., Hariharan, V., Chelladurai, S.J.S., Rajeshkumar, G., Gnanasekaran, S., Sivananthan, S., Debtera, B. (2022). Investigation on mechanical and wear behaviors of LM6 aluminium alloy-based hybrid metal matrix composites using stir casting process. *Advances in Materials Science and Engineering*, Vol. 2022, 4116843. https://doi.org/10.1155/2022/4116843
10. Gonfa, B.K., Sinha, D., Vates, U.K., Badruddin, I.A., Hussien, M., Kamangar, S., Singh, G.K., Ahmed, G.M.S., Kanu, N.J., Hossain, N. (2022). Investigation of mechanical and tribological behaviors of aluminum based hybrid metal matrix composite and multi-objective optimization. *Materials*, Vol. 15(16), 5607. https://doi.org/10.3390/ma15165607
11. Talabi, H., Ojomo, A., Folorunsho, O.E., Akinfolarin, J., Pradeep Kumar, J., Mohan, R.R., Akinwande, A.A., Kumar, M.S. (2023). Development of hybrid aluminium alloy composites modified with locally sourced environmental wastes. *Advances in Materials and Processing Technologies*, Vol. 9(3), pp. 742–759. https://doi.org/10.1080/2374068X.2022.2096831
12. Mourad, A.H.L., Christy, J.V., Krishnan, P.K., Mozumder, M.S. (2023). Production of novel recycled hybrid metal matrix composites using optimized stir squeeze casting technique. *Journal of Manufacturing Processes*, Vol. 88, pp. 45–58. https://doi.org/10.1016/j.jmapro.2023.01.040
13. Moustafa, E.B., Taha, M.A. (2023). The effect of mono and hybrid additives of ceramic nanoparticles on the tribological behavior and mechanical characteristics of an Al-based composite matrix produced by friction stir processing. *Nanomaterials*, Vol. 13(14), 2148. https://doi.org/10.3390/nano13142148
14. Ng, L.F., Yahya, M.Y., Muthukumar, C., Woo, X.J., Muhaimin, A.H., Majid, R.A. (2023). Mechanical characterization of aluminum sandwich structures with woven-ply pineapple leaf/glass fiber-reinforced hybrid composite core. *Journal of Natural Fibers*, Vol. 20(1), 2160404. https://doi.org/10.1080/15440478.2022.2160404
15. Abd El-baky, M.A., Awd Allah, M.M., Kamel, M., Abdel-Aziem, W. (2023). Fabrication of glass/jute hybrid composite over wrapped aluminum cylinders: an advanced material for automotive applications. *Fibers and Polymers*, Vol. 24(1), pp. 143–155. https://doi.org/10.1007/s12221-023-00116-9
16. Abushanab, W.S., Moustafa, E.B., Goda, E.S., Ghandourah, E., Taha, M.A., Mosleh, A.O. (2023). Influence of vanadium and niobium carbide particles on the mechanical, microstructural, and physical properties of AA6061 aluminum-based mono-and hybrid composite using FSP. *Coatings*, Vol. 13(1), 142. https://doi.org/10.3390/coatings13010142
17. Shahabaz, S.M., Mehrotra, P., Kalita, H., Sharma, S., Naik, N., Noronha, D.J., Shetty, N. (2023). Effect of Al_2O_3 and SiC nano-fillers on the mechanical properties of carbon fiber-reinforced epoxy hybrid composites. *Journal of Composites Science*, Vol. 7(4), 133. https://doi.org/10.3390/jcs7040133
18. Bharathi, P., Kumar, T.S. (2023). Mechanical characteristics and wear behaviour of Al/SiC and Al/SiC/B_4C hybrid metal matrix composites fabricated through powder metallurgy route. *Silicon*, Vol. 15(10), pp. 4259–4275. https://doi.org/10.1007/s12633-023-02347-0
19. Sathish, S., Raj, S.S., Nair, A., Sundaraselvan, S. (2024). Investigation on mechanical properties of aluminum hybrid matrix composites reinforced with fly ash and titanium diboride using stir casting technique. *Materials Research Express*, Vol. 11, 076523. https://doi.org/10.1088/2053-1591/ad6238
20. Khoshaim, A.B., Moustafa, E.B., Alazwari, M.A., Taha, M.A. (2023). An Investigation of the mechanical, thermal and electrical properties of an AA7075 alloy reinforced with hybrid ceramic nanoparticles using friction stir processing. *Metals*, Vol. 13(1), 124. https://doi.org/10.3390/met13010124
21. Chandel, R., Sharma, N., Bansal, S.A. (2021). A review on recent developments of aluminum-based hybrid composites for automotive applications. *Emergent Materials*, Vol. 4, pp. 1243–1257. https://doi.org/10.1007/s42247-021-00186-6
22. Lawate, D.N., Shinde, S.S., Jagtap, T.S. (2016). Study of process parameters in stir casting method for production of particulate composite plate. *International Journal of Innovations in Engineering Research and Technology*, Vol. 3(1), pp. 1–5.